Advanced Imaging for Down-Looking Contactless GPR Systems

D. Comite [1], F. Murgia [1], I. Catapano [2], F. Soldovieri [2], and A. Galli [1]

[1] Department of Information Engineering, Electronics and Telecommunications
Sapienza University of Rome, via Eudossiana 18, 00184, Rome, Italy
davide.comite, federica.murgia, alessandro.galli@uniroma1.it

[2] Institute for Electromagnetic Sensing of the Environment (IREA)
National Research Council of Italy (CNR), via Diocleziano 328, 80124, Naples, Italy
catapano.i, soldovieri.f@irea.cnr.it

Abstract ─ This paper investigates the performance of an advanced imaging procedure for ground penetrating radar (GPR) operating in contactless configuration, i.e., when data are collected at variable distances from the air-soil interface. A data processing procedure is presented, based on an advanced implementation of a microwave tomographic approach. This improved version, recently proposed by the authors, is able of accounting for the near-field distribution generated by a directional transmitting antenna. The effectiveness of the procedure is shown by processing numerical data, which are obtained by suitably implementing a realistic system on a full-wave commercial simulator. Metallic canonical objects are considered to compare the reconstruction capabilities of the proposed algorithm with respect to more conventional procedures, as well as to assess the role of the antenna distance from the air-soil interface.

Index Terms ─ Contactless configuration, GPR, inverse scattering, microwave imaging.

I. INTRODUCTION

Detection and reconstruction of shallow-buried targets by means of Ground Penetrating Radar (GPR) systems are highly desirable for several applications, such as demining and planetary exploration as well as for a wide class of non-destructing analyses [1], [2]. Several algorithms have been developed in the last two decades for an effective representation of the raw data collected by means of GPR systems [2]. As concerns the linear microwave tomography (MT), a number of approaches have been proposed [1], which have shown to be capable of providing effective 2-D and 3-D reconstructions (see, e.g., [3], [4], and references therein) in many real situations (e.g., archeology and structural diagnosis) and in different measurement configurations [1], [5]. Several nonlinear algorithms have also been designed [2], based on conventional regularization procedures as well as on *adhoc* strategies able to deal with the occurrence of local minima (i.e., false solutions), in the inversion process [6].

In standard implementations of the inversion and post-processing procedures, the source activating the scattering phenomenon is usually modeled as a filamentary electric current, or as an impinging plane wave, assuming, in this last case, the transmitter located in the far field with respect to the investigated region. In this context, several efforts have already been focused on the possibility of taking into account the pattern of the antenna that illuminates the considered object. A first insight into the role played by the antenna pattern for linear MT inversion algorithm has been provided in [7], whereas in [8] an extension of a migration algorithm, capable to account for the radiation pattern of an ideal antenna for multi-component GPR data, has been designed. A diffraction tomography algorithm accounting for the incident near-field distribution has also been proposed in [9]. For some applications, such as road prospecting [1] or planetary exploration [10], [11], the capability of collecting and elaborating data in contactless configuration, i.e., when the system is located at a distance from the air-soil interface at least comparable with the operating wavelengths, is highly desirable. In this frame, the theoretical solutions, which account for the presence of the interface, are based on a spectral decomposition of the Green's function of the problem (see, e.g., [4], [5]).

We investigate here the performance achievable by a linear MT approach, when the radiative features of a directional wide-band antenna, working in contactless configuration, are modeled in an *advanced* algorithm.

As a reference case, we focus our analysis on a directional system as that proposed for the WISDOM rover, in the framework of the ExoMars planetary mission [10], which requires a compact wide-band radiator to focus electromagnetic signals in the ground. A wide-band (0.5–3 GHz) printed Vivaldi antenna operating at a certain distance from the air-soil interface is thus considered as an effective and reliable solution for both *Tx* and *Rx* system [10]. We exploit here an efficient and reliable customized

Submitted On: July 3, 2017
Accepted On: May 13, 2018

numerical implementation based on *CST Microwave Studio*, widely tested by the authors to simulate actual GPR scenarios involving also commercial systems [11].

In this framework, the authors have already evaluated the radiative features of the Vivaldi antenna working in ground-coupled configurations [12], and including the near-field distribution of the antenna in the inversion algorithm. To this aim, various comparisons for the reconstructions, generated by modeling the scattering phenomenon as occurring in a homogeneous medium, were performed.

In the following, we propose a more general implementation of our advanced procedure, which removes the assumption of homogeneous medium and allows us to account for the presence of the air-soil discontinuity, positioning the antenna not in contact with the interface. In particular, we discuss the effects on the reconstruction results by considering different targets having canonical shape, with the directional antenna placed at variable distances from the interface. A frequency range from 0.5 to 3 GHz is considered.

II. IMAGING ALGORITHMS

We assume in our analysis a two half-space model with a GPR working in monostatic configuration placed at a distance D_g from the interface between air and a nonmagnetic and lossless dielectric medium (see Fig. 1), having permittivity ε_r = 3.2, which effectively models a Martian-like sandy subsoil (see [11] and references therein). Similar values of the permittivity can also represent realistic wet soils having moisture content of about 5-10%. We consider here the direct solution of the scattering problem on a 2-D transverse plane (i.e., the *xy* plane in Fig. 1, half-cutting the buried object). Since the numerical scattering data are obtained by means of a 3D implementation and solution of the GPR scenario, to reduce the problem to a 2D scalar implementation, but preserving the directional features of the illumination, we consider the dominant component (i.e., the *x*-directed, for this case) of the field radiated by the Vivaldi antenna on the reference vertical plane. This allows for neglecting the dyadic nature of the wave/material interactions, and to deal with a simplified 2D scalar case.

The imaging procedure is formulated as a linear inverse scattering problem in the frequency domain [1] and the physical-optics (PO) approximation is adopted [13]. Accordingly, at each angular frequency ω and for each position of the antenna along the scanline, the scattered field at the receiver can be modeled as follows:

$$E_s(x_R,\omega) = -j\omega\mu_0 \int_\Gamma G(x_R;\mathbf{r}';\omega)\, J_{PO}(x_T;\mathbf{r}';\omega) d\Gamma', \quad (1)$$

where $E_s(x_R,\omega)$ denotes the complex scattered electric field for $f = \omega/(2\pi)$, probed at x_R (equal here to the source position x_T); k_b is the wavenumber in the background lower half-space, G is the scalar Green's function of the problem, Γ is the contour of the scattering object (unknown of the problem). J_{PO} is the physical-optics surface current density flowing on the metallic contour of the object, related to the incident magnetic field in the lower half-space (in absence of scatterers) [2]. To account for the presence of the air-soil interface, we exploit the following spectral representation of the Green's function [1]:

$$G(x_R,\mathbf{r}') = \frac{-j}{2\pi}\int_{-\infty}^{\infty} \frac{e^{-jk_{yb}y'} e^{-jk_{y0}D_g}}{k_{y_0}+k_{y_b}} e^{-jk_y(x_R-x')} dk_x, \quad (2)$$

being $k_{y0} = \sqrt{k_0^2 - k_x^2}$ and $k_{yb} = \sqrt{k_s^2 - k_x^2}$.

To recover the unknown object contour, we follow the procedure outlined in [14]: thus (1) is discretized, inverted, and regularized through the truncated singular value decomposition (TSVD) approach [1], [7].

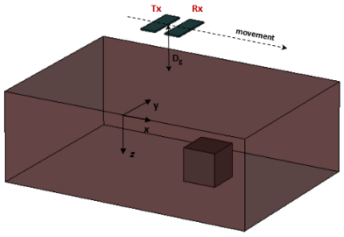

Fig. 1. 3D GPR reference scenario: a canonical object having dimension comparable with respect to the probing wavelengths is buried in the shallow region made by a dielectric half-space. The GPR is placed at a distance D_g from the air-soil interface.

In *standard* implementations, the evaluation of the scattered field is carried out by inserting (2) in (1). The impinging field on the object (that give rises to the currents J_{PO}) is assumed as that generated by a *line source*; due to reciprocity, the incident field is expressed by means of a spectral representation similar to (2). This can be accomplished by exploiting a simple point-matching procedure representing each pixel by means of a proper set of basis functions [3], [5].

To account for the actual near-field distribution radiated by the antenna we have generalized the *advanced* procedure outlined in [12]: the field radiated by a Vivaldi antenna and simulated with CST, as well as the Green's function of the problem, are exported and suitably inserted in (1), by considering both amplitude and phase of each sample in the frequency band of interest. Once that a linear discrete operator is obtained, the TSVD regularization scheme is adopted [1], [2] to retrieve the unknown Γ.

We mention that the proposed *advanced* procedure allows for sensibly mitigating the computational burden requested to deal with the frequency-domain spectral representation in (2). In fact, the wideband nature of the problem is alternatively faced here exploiting a time-domain solution of both incident field and Green's function of the problem. Thus, the FFT is applied to the impinging and scattered signals to generate the linear operator to be regularized and inverted.

III. RESULTS AND DISCUSSION

To assess and compare the capability of the

proposed advanced algorithm, which accounts for the actual field radiated by the antenna, we compare the imaging results with those provided by the MT approach as implemented in the standard way, i.e., by modeling the incident field as radiated by a filamentary current through the spectral representation of (2).

A. Canonical shapes for a fixed antenna height

The distance between the antenna and the interface has been fixed to D_g = 20 cm. The reconstruction capabilities of the algorithms are tested on four different metallic canonical configurations: *i*) a cube whose flat face is normal to the direction of illumination; *ii*) the inscribed sphere (diameter as the cube side); *iii*) a square-base pyramid; and *iv*) a cube rotated of 45°.

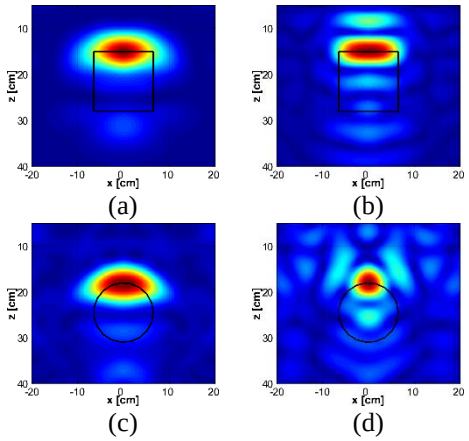

Fig. 2. Tomographic reconstructions of targets buried at a distance d = 15 cm from the air-sand interface, with the GPR antenna raised at D_g = 20 cm (cf. Fig. 1). (a) *Metallic cube* (side 13 cm) imaged with a *standard* implementation of the algorithm; (b) as in (a), with our *advanced* implementation, accounting for the actual near-field radiated by a Vivaldi antenna; (c) *metallic sphere* (diameter 13 cm) with the *standard* implementation; (d) as in (c), with our *advanced* implementation. T = −25 dB and the black-line profiles represent the *zx* section of the scatterers.

In Figs. 2 (a) and (b), the reconstruction obtained for the metallic cube (see caption for details) is reported for both the implementations. One can clearly recognize the signature relevant to the target. The upper side of the cube is better resolved by the advanced implementation, which provides also an improved focusing of the illuminated side of the object. The same observations apply to the profile presented in Figs. 2 (c) and (d), regarding the reconstruction of the metallic spherical object. However, the reconstruction improvements achievable in such contactless geometries are less evident with respect to the ground-coupled configuration (see also [12]). This is mainly due to the reduced synthetic aperture provided by the systems when $D_g \neq 0$. We mention that the advanced reconstruction shows enhanced resolution but appears a bit more noisy around the central spot. This is due to the behavior of the singular values (similar to the one reported in [12]), which, for a fixed T, forces the advanced approach to deal with smaller, hence possibly noisier, values.

We note that, as also discussed in [12], the improvement in focusing the top side of the illuminated objects are not related to the total number of singular values comprised in the inversion scheme, but to the more accurate description of the directional features of the illuminating field. In fact, due to the smaller synthetic aperture provided by the Vivaldi antenna, even a smaller number of singular values are accounted for with the advanced scheme by thresholding the whole set to T = –25 dB with respect to maximum value.

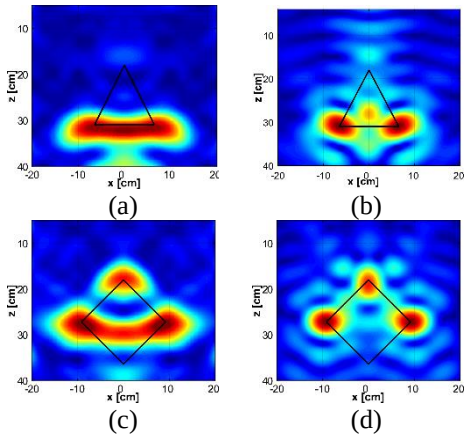

Fig. 3. As in Fig. 2, for other target shapes. (a) A *metallic pyramid* (base 13 cm, height 13 cm), buried at d = 15 cm, with the standard algorithm; (b) as in (a), with the advanced one; (c) a *metallic cube* (d = 18 cm) as in Figs. 2 (a,b), but *rotated of 45°*, with the standard implementation; (d) as in (c), with the advanced one; T = −25 dB.

In Figs. 3 (a) and (b) the same comparisons are presented for a metallic pyramid scatterer. Also in this case, the reconstruction capabilities of the advanced implementation are manifestly improved, since the two main edges giving the main contribution to the scattered field at the bottom of the pyramid are better resolved and reconstructed. Note that the bottom side of the pyramid is not illuminated and cannot give an appreciable contribution to the scattered field (the bottom profile in Fig. 3 (a) is fictitious and determined by the absence of adequate resolution). In addition, the spot visible at the bottom of the frame is determined by interference between two dominant scattering phenomena. It becomes weaker for a pyramid having a larger base. In Figs. 3 (c) and (d) the enhanced capabilities of the advanced procedure in locating and reconstructing the edges of the metallic rotated cube are also clearly visible. The presence of an elongated edge makes it visible with respect to vertex of the pyramid.

B. Effect of different antenna heights

Here we show the reconstructions for different values of D_g, in order to assess the informative contents provided by both the standard and advanced procedure as the antenna/interface distance gradually increases.

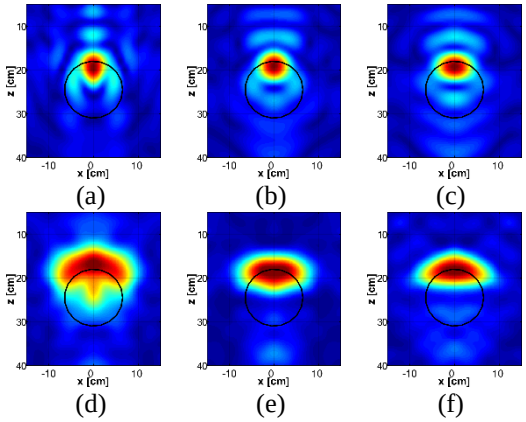

Fig. 4. Reconstructions of a metallic sphere buried at d = 18 cm from the interface, as in Figs. 2 (a, b), for different values of D_g: (a)-(c) advanced implementation for D_g = 0, 10, 25 cm, respectively; (d)-(f) as in (a)-(c) but with standard implementation; $T = -25$ dB.

In Figs. 4 (a)-(c) and (d)-(f), the reconstructions of a metallic sphere are presented for three different values of D_g (see captions) by considering both the implementations. From the analysis of Fig. 4, in conjunction with the results shown in Figs. 2 (a)-(b) and in Figs. 2 (c)-(d), one can clearly assess the improved imaging capabilities of the advanced algorithm, whose performance slightly degrade as D_g is increased. This can be related to the smaller synthetic aperture (i.e., the underlying angle-of-view) not compensated by an increasing dimension of the measurement line (kept constant for all the simulations to 75 cm).

IV. CONCLUSION

We have specifically discussed the performance of a microwave tomographic approach based on the PO approximation and accounting for the effective radiation behavior of a directional GPR antenna working in contactless configuration. The actual spatial distribution of the incident field and Green's functions, for variable distances between the antenna and the air/soil interface, has suitably been included in the numerical algorithm.

We have shown that, when a specific directive antenna is employed, the proposed advanced implementation can be beneficial to the quality of the reconstruction, especially for metallic objects with sharp edges.

The improvements in the spatial reconstructions of the targets have resulted to be generally significant. On the other hand, we have also shown that, when the antenna height from the interface gradually increases, the imaging becomes less informative on the target profiles, even if correct detection and localization are achieved.

REFERENCES

[1] R. Persico, *Ground Penetrating Radar: Inverse Scattering and Data Processing*. Wiley, 2014.

[2] M. Pastorino, *Microwave Imaging*. Wiley, 2010.

[3] G. Leone and F. Soldovieri, "Analysis of the distorted Born approximation for subsurface reconstruction: Truncation and uncertainties effects," *IEEE Trans. Geosci. Rem. Sens*., vol. 41, no. 1, pp. 66-74, Jan. 2003.

[4] T. B. Hansen and P. M. Johansen, "Inversion scheme for ground penetrating radar that takes into account the planar air-soil interface," *IEEE Trans. Geosci. Remote Sens.*, vol. 38, no. 1, pp. 496-506, Jan. 2000.

[5] R. Persico, "On the role of measurement configuration in contactless GPR data processing by means of linear inverse scattering," *IEEE Trans. Antennas Propag.*, vol. 54, no. 7, pp. 2062-2071, July 2006.

[6] M. Salucci, G. Olivieri, and A. Massa, "GPR prospecting through an inverse-scattering frequency-hopping multi-focusing approach," *IEEE Trans. Geosci. Remote Sens.*, vol. 53, no. 12, pp. 6573-6592, Jan. 2015.

[7] F. Soldovieri, R. Persico, and G. Leone, "Effect of source and receiver radiation characteristics in subsurface prospecting within the distorted Born approximation," *Radio Sci*., vol. 40, pp. 1-13, June 2005.

[8] R. Streich and J. van der Kruck, "Accurate imaging of multicomponent GPR data based on exact radiation patterns," *IEEE Trans. Geosci. Remote Sens.*, vol. 45, pp. 93-103, Jan. 2007.

[9] C. Dourthe, C. Pichot, J. Y. Dauvignac, and J. Cariou, "Inversion algorithm and measurement system for microwave tomography of buried object," *Radio Sci.*, vol. 35, pp. 1097-1108, Apr. 2000.

[10] V. Ciarletti, et al., "WISDOM GPR designed for shallow and higher solution sounding of the martian subsurface," *Proc. IEEE*, vol. 99, pp. 825-836, May 2011.

[11] G. Valerio, et al., "GPR detectability of rocks in a Martian-like shallow subsoil: A numerical approach," *Planet. Space Sci*., vol. 62, pp. 31-44, 2012.

[12] D. Comite, A. Galli, I. Catapano, and F. Soldovieri, "The role of the antenna radiation pattern in the performance of a microwave tomographic approach for GPR imaging," *IEEE J. Sel. Topics Appl. Earth Observ. Remote Sens.*, vol. 10, no. 10, pp. 4337-4347, Oct. 2017.

[13] R. Pierri, A. Liseno, R. Solimene, and F. Soldovieri, "Beyond physical optics SVD shape reconstruction of metallic cylinders," *IEEE Trans. Antennas Propag.*, vol. 54, no. 2, pp. 655-665, Feb. 2006.

[14] F. Soldovieri, et al., "GPR estimation of the geome-trical features of buried metallic targets in testing conditions," *Prog. Electromagn. Res. B*, vol. 49, pp. 339-362, 2013.